




Article

Nipalarsite, Ni₈Pd₃As₄, a new platinum-group mineral from the Monchetundra Intrusion, Kola Peninsula, Russia

Tatiana L. Grokhovskaya¹, Oxana V. Karimova¹, Anna Vymazalová^{2*} , František Laufek², Dmitry A. Chareev^{3,4,5}, Elena V. Kovalchuk¹, Larisa O. Magazina¹ and Victor A. Rassulov⁶

¹Institute of Geology of Ore Deposits, Petrology, Mineralogy and Geochemistry Russian Academy of Sciences, Staromonetnyi per. 35, Moscow 119017, Russia; ²Czech Geological Survey, Geologická 6, 152 00 Prague 5, Czech Republic; ³Institute of Experimental Mineralogy, Russian Academy of Sciences Akademica Osypyna st., 4, 142432, Chernogolovka, Moscow region, Russia; ⁴Institute of Physics and Technology, Ural Federal University, Ekaterinburg, Russia; ⁵Institute of Geology and Petroleum Technologies, Kazan Federal University, Kazan, Russia; and ⁶All-Russian Scientific Research Institute of Mineral Resources, Staromonetny per. 31, Moscow 119017, Russia

Abstract

Nipalarsite, Ni₈Pd₃As₄, is a new platinum-group mineral discovered in the sulfide-bearing orthopyroxenite of the Monchetundra layered intrusion, Kola Peninsula, Russia (67°52′22″N, 32°47′60″E). Nipalarsite forms anhedral grains (5–80 μm in size) in intergrowths with sperrylite, kotulskite, hollingworthite, isomertieite, menshikovite, parlarstanide, nielsenite and monchetundtraite enclosed in pentlandite, anthophyllite, actinolite and chlorite. Nipalarsite is brittle, has a metallic lustre and a grey streak. In plane-polarised light, nipalarsite is light grey with a blue tinge. Reflectance values in air (in %) are: 46.06 at 470 nm, 48.74 at 546 nm, 50.64 at 589 nm and 54.12 at 650 nm. Values of VHN₂₀ fall between 400.5 and 449.2 kg.mm⁻², with a mean value of 429.9 kg.mm⁻², corresponding to a Mohs hardness of ~4. The average result of 27 electron microprobe wavelength dispersive spectroscopy analyses of nipalarsite is (wt.%): Ni 44.011, Pd 28.74, Fe 0.32, Cu 0.85, Pt 0.01, Au 0.05, As 25.42, Sb 0.05, Te 0.39, total 99.85. The empirical formula (normalised to 15 atoms per formula unit) is: (Ni_{8.10}Fe_{0.06})Σ8.16(Pd_{2.94}Cu_{0.18})Σ3.12(As_{3.68}Te_{0.03})Σ3.71 or, ideally, Ni₈Pd₃As₄. Nipalarsite is cubic, space group *Fm*3̄*m*, with *a* = 11.4428(9) Å, *V* = 1498.3(4) Å³ and *Z* = 8. The strongest lines in the powder X-ray diffraction pattern of synthetic Ni₈Pd₃As₄ [*d*, Å (*I*) (*hkl*)] are: 2.859(10)(004), 2.623(6)(313), 2.557(6)(024), 2.334(11)(224), 2.201(35)(115,333), 2.021(100)(044), 1.906(8)(006,244) and 1.429(7)(008). The crystal structure was solved and refined from the single-crystal X-ray diffraction data of synthetic Ni₈Pd₃As₄. The relation between natural and synthetic nipalarsite is illustrated by an electron back-scattered diffraction study of natural nipalarsite. The density calculated on the basis of the empirical formula of nipalarsite is 9.60 g.cm⁻³. The mineral name corresponds to the three main elements: Ni, Pd and As.

Keywords: nipalarsite, platinum-group mineral, Ni₈Pd₃As₄ phase, electron-microprobe data, reflectance data, X-ray diffraction data, crystal structure, Monchetundra layered intrusion, Russia

(Received 20 July 2019; accepted 29 October 2019; Accepted Manuscript published online: 5 November 2019; Associate Editor: Irina O Galuskina)

Introduction

Nipalarsite, Ni₈Pd₃As₄, is a new platinum-group mineral (PGM) species discovered in specimen from the Monchetundra layered intrusion, Kola Peninsula, Russia. The mineral was found in a drill core taken from the borehole 1819 (67°52′22″N, 32°47′60″E) at the depth of 101.3–101.4 m. The mineral was discovered initially as anhedral grains (5–80 μm in size) in polished sections from the bulk sample 1819074 (Grokhovskaya *et al.*, 2009, fig. 3a, c–e). It was described preliminarily as an unnamed phase, Ni₆Pd₂As₃, intergrown with other PGM (UM2003-40-As: NiPd, UM2009-02-As: NiPd, Grokhovskaya *et al.*, 2003, 2009).

A mineral with corresponding chemical composition [(wt.%: Pd 26, Ni 44.6, As 28, total 98.6, with an empirical formula (based on 15 atoms) of Ni_{8.27}Pd_{2.66}As_{4.07})] and XRD data [*d*, Å, *I* (%) (2.28 (3); 2.20 (4); 2.02 (10); 1.931 (3))] was also listed as an unnamed phase Pd₂Ni₆As₃ (UM1986-As: NiPd) from massive cubanite–talnakhite ores of the Talnakh and Norilsk deposits, Russia (Genkin *et al.*, 1981; Genkin and Evstigneeva, 1986). Previously, Gervilla *et al.* (1994) reported, that it could represent a Ni-rich extension of the (Pd,Ni)₈As₃ solid-solution series, end-member of which is a mineral known as stillwaterite Pd₈As₃.

The name of the mineral corresponds to its chemical composition: Ni, Pd and As. Both the mineral and mineral name were approved by the Commission on New Minerals and Mineral Names, IMA (IMA2018-075, Grokhovskaya *et al.*, 2018). The type material is deposited at the Fersman Mineralogical Museum, Russian Academy of Sciences, Leninsky Prospekt 18–2, Moscow 119071, Russia, registration number 5236/1.

*Author for correspondence: Anna Vymazalová, Email: anna.vymazalova@geology.cz

Cite this article: Grokhovskaya T.L., Karimova O.V., Vymazalová A., Laufek F., Chareev D.A., Kovalchuk E.V., Magazina L.O. and Rassulov V.A. (2019) Nipalarsite, Ni₈Pd₃As₄, a new platinum-group mineral from the Monchetundra intrusion, Kola Peninsula, Russia. *Mineralogical Magazine* 83, 837–845. <https://doi.org/10.1180/mgm.2019.70>

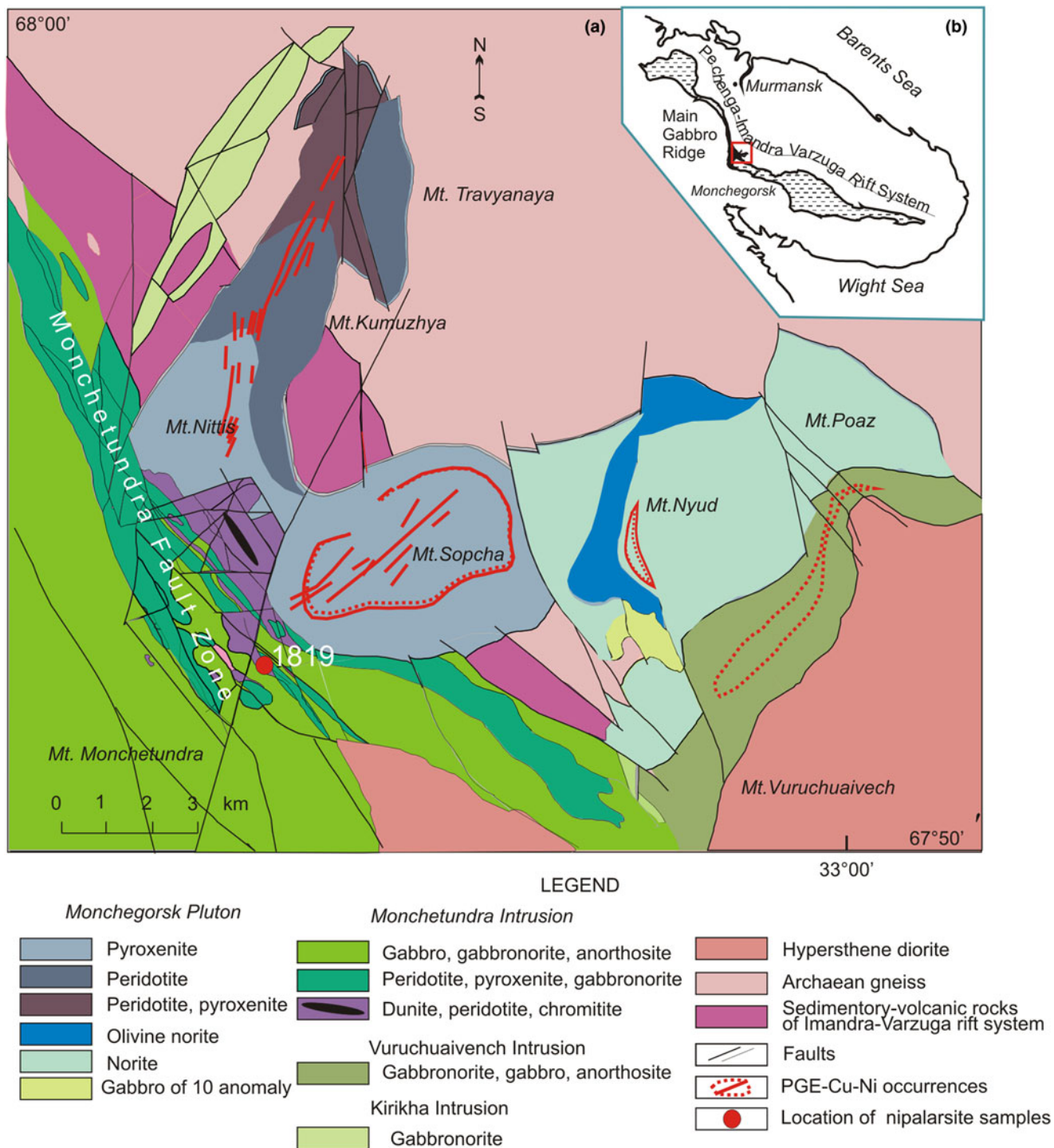


Fig. 1. Simplified geological map of the Monchegorsk Igneous Complex showing the sample location (modified from Grokhovskaya et al., 2003).

The article describes the properties of the mineral and its geological occurrence, along with comments on its potential conditions of formation.

Geological setting, occurrence and associated minerals

The Early Palaeoproterozoic (2504.4 ± 1.5 to 2453 ± 4 Ma) layered intrusions of the Monchegorsk Igneous Complex are located within

the southern inner corner of the Pasvic-Pechenga-Imandra-Varzuga rift-transform system (Amelin et al., 1995; Grokhovskaya et al., 2003; Bayanova et al., 2010). The Monchegorsk Igneous Complex intrudes into gneisses of the Archaean Kola Group and is overlain by volcanics and clastics of Palaeoproterozoic Pechenga-Varzuga Series. The Monchegorsk Igneous Complex consists of the 'Main Gabbro Ridge' massif (including the Monche-, Chuna-, Volche- and Losevy-Tundra intrusions) striking

Table 1 Electron-microprobe analyses of PGM associated with nipalarsite, Monchetundra layered intrusion

Mineral	Mer	Kot	Mon	Mtt	Tel	Lvt	Ism	Mnv	Pls	Pls	Cu ₃ Pt	Nlt	Hlt	Irt	Spt
wt%															
Pd	28.70	45.85	n.d	39.89	42.97	50.99	70.67	48.72	65.55	67.04	4.04	32.35	n.d	n.d	n.d
Pt	1.36	0.81	43.85	n.d	n.d	n.d	0.01	n.d	n.d	n.d	40.92	n.d	22.82	12.48	52.4
Rh	n.d	n.d	n.d	–	–	–	n.d	–	–	–	n.d	–	20.75	5.22	2.01
Ir	–	–	–	–	–	–	–	–	–	–	–	–	n.d	30.55	n.d
Ru	–	–	–	–	–	–	–	–	–	–	–	–	9.94	4.84	n.d
Os	–	–	–	–	–	–	–	–	–	–	–	–	n.d	3.88	n.d
Ag	–	–	–	–	26.62	7.19	n.d	–	–	–	–	–	–	n.d	n.d
Ni	0.02	–	0.50	11.06	n.d	n.d	0.27	17.3	0.53	–	3.25	0.12	–	0.40	0.10
Cu	n.d	–	n.d	0.12	–	0.69	4.05	n.d	0.11	0.59	47.64	64.5	–	n.d	n.d
Au	–	–	–	n.d	0.32	n.d	n.d	–	1.21	5.12	n.d	n.d	–	–	–
Fe	–	–	–	0.23	n.d	–	–	–	0.63	0.81	1.79	1.32	–	0.54	0.12
Sn	–	–	–	n.d	–	–	0.58	–	21.29	11.7	n.d	n.d	–	n.d	n.d
Sb	–	–	–	–	–	–	15.61	–	0.56	n.d	–	–	–	–	–
Te	57.80	53.26	54.84	48.4	24.73	42.06	n.d	–	n.d	–	–	–	–	–	–
Bi	12.12	n.d	n.d	n.d	5.22	n.d	–	–	–	–	–	–	–	–	–
As	n.d	–	–	–	0.06	–	9.52	33.64	7.86	13.87	1.54	n.d	31.95	24.84	43.7
S	–	–	–	–	n.d	–	n.d	n.d	n.d	n.d	–	–	14.69	11.14	0.54
Total	100.00	99.92	99.19	99.70	99.92	100.93	100.71	99.66	97.77	99.13	99.18	98.29	100.15	93.89	98.88
apfu	3	2	3	5	4	25	15	8	7	7	4	4	3	3	3
Pd	1.03	1.01	–	1.98	1.85	13.52	10.04	3.05	4.62	4.58	0.14	0.9	–	–	–
Pt	0.03	0.01	1.02	–	–	–	–	–	–	–	0.76	–	0.27	0.19	0.9
Rh	–	–	–	–	–	–	–	–	–	–	–	–	0.47	0.15	0.07
Ir	–	–	–	–	–	–	–	–	–	–	–	–	–	0.46	–
Ru	–	–	–	–	–	–	–	–	–	–	–	–	0.23	0.14	–
Os	–	–	–	–	–	–	–	–	–	–	–	–	–	0.06	–
Ag	–	–	–	–	1.13	1.88	–	–	–	–	–	–	–	–	–
Ni	–	–	0.04	0.99	–	–	0.07	1.96	0.07	–	0.2	0.01	–	0.02	0.01
Cu	–	–	–	0.01	–	0.31	0.96	–	0.01	0.07	2.71	3.02	–	–	–
Au	–	–	–	–	0.01	–	–	–	0.05	0.19	–	–	–	–	–
Fe	–	–	–	0.02	–	–	–	–	0.09	0.11	0.12	0.07	–	0.03	0.01
Sn	–	–	–	–	–	–	0.07	–	1.35	0.72	–	–	–	–	–
Sb	–	–	–	–	–	–	1.94	–	0.03	–	–	–	–	–	–
Te	1.72	0.98	1.94	2	0.89	9.3	–	–	–	–	–	–	–	–	–
Bi	0.22	–	–	–	0.11	–	–	–	–	–	–	–	–	–	–
As	–	–	–	–	–	–	1.92	2.99	0.79	1.35	0.07	–	0.98	0.96	1.96
S	–	–	–	–	–	–	–	–	–	–	–	–	1.06	1.01	0.06

Abbreviations: Mer – merenskyite, Kot – kotulskite, Mon – moncheite, Mtt – monchetundraite, Tel – telargpalite, Lvt – lukkulaisvaaraite, Ism – isomertieite, Mnv – menshikovite, Pls – palarstanide, Nlt – nielsenite, Hlt – hollingworthite, Irt – irarsite, Spt – sperrylite; n.d – not detected; ‘–’ not analysed; apfu – atoms per formula unit.

NW to SE, and the Monchegorsk Pluton (Fig. 1a,b). Ultramafic cumulates prevail in the Monchegorsk Pluton whereas intrusions of Main Gabbro Ridge are composed mainly of mafic, and to a lesser extent of ultramafic cumulates.

The Monchetundra layered intrusion consists of a lower ultrabasic zone of dunite, peridotite and pyroxenite (100–300 m thick); a middle zone of rhythmically layered pyroxenite, olivine pyroxenite, norite and gabbronorite (300–400 m thick), and an upper zone of gabbronorite and gabbronorite-anorthosite (800–1000 m thick). The reef-type platinum-group element (PGE) mineralisation (up to 3–5 ppm Pt + Pd) was discovered within a rhythmically layered zone (Grokhovskaya *et al.*, 2003; 2009).

The Monchetundra intrusion and Monchegorsk Pluton join along the Monchetundra Regional Fault expressed by an extremely permeable shear-zone striking SE–NW. The Monchetundra Regional Fault consists of a lot of steeply dipping faulted slices represented by more- or less-altered rocks of the Monchetundra intrusion, ranging from dunite and peridotite, to pyroxenite, norite and gabbronorite. Low-sulfide PGE mineralisation is located in tectonised chromite-bearing peridotite, pyroxenite and norite, which features highly variable thicknesses (from 1 to 100 m) and PGE contents (from 1–3 to 20 ppm Pt + Pd). More

than fifty PGM species have been found in this shear zone including nipalarsite (Grokhovskaya *et al.*, 2009).

The host rocks of the samples investigated are represented by orthopyroxene cumulates and consist of orthopyroxene, olivine, augite and plagioclase, sometimes totally replaced by anthophyllite, actinolite, Mg-hornblende, biotite–phlogopite-group and chlorite-group minerals with minor chromite, ilmenite and magnetite. Disseminated sulfides include pentlandite, violarite, heazlewoodite, chalcopyrite, chalcocite and pyrrhotite with some accessory minerals. The most common PGM are sperrylite, kotulskite, moncheite, merenskyite, isomertieite, telluropalladinite, keithconnite, hollingworthite, irarsite, stibiopalladinite, lukkulaisvaaraite, nipalarsite, menshikovite, telargpalite, monchetundraite, palarstanide, nielsenite and Cu₃Pt, listed in approximate order of abundance. The electron-microprobe data associated with nipalarsite are given in Table 1.

Nipalarsite typically occurs as a part of complex polymineralic PGM intergrowths attached to pentlandite and enclosed in amphiboles and chlorite (Fig. 2a–f). Nipalarsite was found in polished sections and heavy-mineral concentrates ranging in size from 3.0 to 80 µm. It forms anhedral and subhedral grains intergrown with sperrylite, kotulskite, hollingworthite, isomertieite, palarstanide, monchetundraite and pentlandite (Fig. 2a,b).

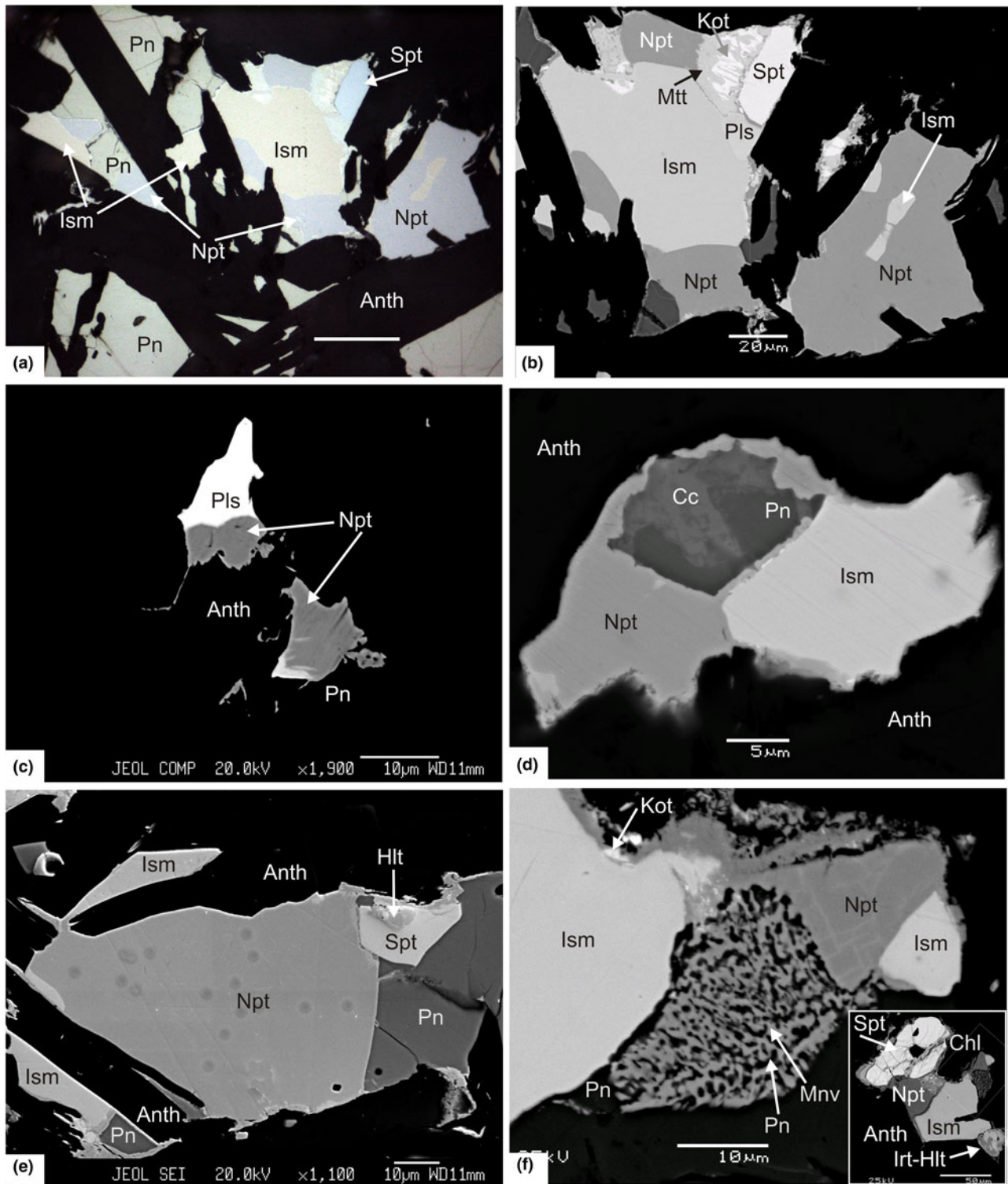


Fig. 2. Reflected light (a) and back-scattered electron (b–f) images of nivalarsite (Npt) and associated minerals from the Monchetundra intrusion. (a, b) Association of nivalarsite, isomertieite (Ism), sperrylite (Spt), palarsitanide (Pls) and kotulskite (Kot), replaced by monchetundraite (Mtt) and pentlandite (Pn); (c) two small grains of nivalarsite (used for EBSD analysis) intergrown with palarsitanide embedded in anthophyllite (Anth); (d) nivalarsite (used for EBSD analysis), isomertieite and pentlandite replaced by chalcocite (Cc); (e) polyphase PGMs represented by nivalarsite, isomertieite, sperrylite and hollingworthite, attached to pentlandite enclosed in anthophyllite and chlorite (Chl); (f) association of nivalarsite with isomertieite, menshikovite (Mnv) and pentlandite (Pn); inset in the right corner – general view of polyphase intergrowth of nivalarsite with other PGMs.

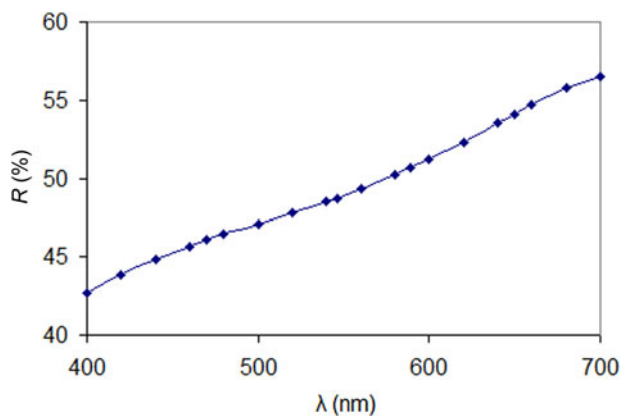
The genetic link between nivalarsite and other PGM is not apparent: in some cases nivalarsite forms its own grains attached to pentlandite (Fig. 2a,e), after pentlandite (Fig. 2d), or in one

case possibly menshikovite and pentlandite formed symplectites then replaced by nivalarsite, or menshikovite occurred after nivalarsite in a pentlandite matrix (Fig. 2f). An advanced deposition

Table 2. Reflectance data (%) for nipalarsite in air.

λ (nm)	<i>R</i> (%)	λ (nm)	<i>R</i> (%)	λ (nm)	<i>R</i> (%)
400	42.72	520	47.81	620	52.33
420	43.82	540	48.52	640	53.52
440	44.81	546	48.74	650	54.12
460	45.66	560	49.3	660	54.7
470	46.06	580	50.2	680	55.74
480	46.43	589	50.64	700	56.46
500	47.12	600	51.21		

The values required by the Commission on Ore Mineralogy are given in bold.

**Fig. 3.** Reflectance data for nipalarsite in air. The reflectance values (*R*, %) are plotted versus wavelength (λ , nm).

of pentlandite in relation to the PGM is indicated in Fig. 2e, as the pentlandite is fractured and its cracks do not propagate into the adjacent nipalarsite.

Physical and optical properties

Nipalarsite is opaque, with metallic lustre, and brittle. Its powder has a grey streak. In plane-polarised reflected light the mineral is light grey with a blue tinge; in intergrowths associated with sperrylite it has a lilac tint. Reflectance values of nipalarsite were measured in air using an MSFU-312 microspectrophotometer (LOMO, Russia) with a WTiC standard (R589 in air = 48.7%). Reflectance data for natural nipalarsite are given in Table 2 and illustrated in Fig. 3. Values of VHN_{20} fall between 400.5 and 449.2 $\text{kg}\cdot\text{mm}^{-2}$, with a mean value of 429.9 $\text{kg}\cdot\text{mm}^{-2}$, corresponding to a Mohs hardness of ~ 4 . The density calculated on the basis of the empirical formula is $9.60 \text{ g}\cdot\text{cm}^{-3}$.

Chemical composition

Chemical analyses were performed with a Jeol 8200 electron probe microanalyser in wavelength dispersive spectroscopy (WDS) mode using an electron beam diameter focused to 1–2 μm , with an accelerating voltage of 20 kV and a beam current of 20 nA on the Faraday cup. Pure Ni, Pd, Pt, Au metals, and FeS_2 , CuFeS_2 , PbS , GaAs , Sb_2S_3 and AuTe_2 were used as standards. Concentrations were quantified on the $K\alpha$ lines for Cu, Fe, Ni; $L\alpha$ lines for Au, Pd, Pt, As, Te, Sb; and $M\alpha$ line for Pb.

Nipalarsite has a fairly constant composition, WDS analyses of representative grains are given in Table 3. The average result of 27 electron microprobe WDS analyses of nipalarsite is (wt.%): Ni 44.01, Pd 28.74, Fe 0.32, Cu 0.85, Pt 0.01, Au 0.05, As 25.42, Sb 0.05, Te 0.39, total 99.85. The empirical formula (normalised to 15 atoms per formula unit) for nipalarsite is: $(\text{Ni}_{8.10}\text{Fe}_{0.06})_{\Sigma 8.16}(\text{Pd}_{2.94}\text{Cu}_{0.18})_{\Sigma 3.12}(\text{As}_{3.68}\text{Te}_{0.03})_{\Sigma 3.71}$, ideally, $\text{Ni}_8\text{Pd}_3\text{As}_4$, and for the synthetic analogue (average of nine analyses) is $\text{Ni}_{8.20}\text{Pd}_{2.80}\text{As}_{4.00}$.

Table 3. Electron-microprobe analyses of nipalarsite and its synthetic analogue*.

Grain No.	gr1-1	gr1-4	gr1-6	gr1-8	gr1-10	gr1-12	gr2-2	gr2-5	gr2-8	gr3-4	gr3-5	gr5-18	Synth. <i>n</i> = 9
wt.%													
Ni	45.22	43.26	44.70	45.59	43.45	43.28	44.32	43.15	43.70	42.67	43.47	44.58	44.78
Pd	27.62	29.35	28.33	27.52	29.42	29.23	28.20	30.26	30.08	29.58	28.92	26.98	27.73
Pt	0.00	0.05	0.01	n.d.	n.d.	0.08	n.d.	n.d.	n.d.	n.d.	n.d.	n.d.	
Au	0.07	n.d.	0.15	0.19	n.d.	0.09	0.03	0.21	n.d.	n.d.	n.d.	n.d.	
Fe	0.26	0.04	0.19	0.11	0.10	0.24	0.07	0.07	0.13	0.87	0.81	0.54	
Cu	0.34	1.81	0.39	0.29	1.93	1.10	0.47	0.53	0.21	1.05	0.50	1.68	
Pb	0.02	0.05	n.d.	0.03	n.d.	n.d.	n.d.	0.03	n.d.	n.d.	0.03	0.07	
As	25.94	25.06	25.86	25.76	24.74	25.13	25.16	25.50	25.43	25.19	25.10	25.05	27.90
Sb	0.04	0.04	0.08	0.06	0.07	0.07	0.04	0.04	0.09	n.d.	n.d.	n.d.	
Te	n.d.	n.d.	n.d.	n.d.	n.d.	n.d.	1.08	1.44	0.85	0.05	0.88	0.41	
Total	99.51	99.66	99.70	99.56	99.69	99.23	99.37	101.23	100.48	99.4	99.72	99.30	100.41
Atoms per formula unit (based on 15 atoms)													
Ni	8.33	8.03	8.26	8.40	8.05	8.07	8.25	7.98	8.10	7.94	8.07	8.21	8.20
Pd	2.81	3.00	2.89	2.80	3.01	3.01	2.89	3.09	3.07	3.04	2.96	2.74	2.80
Pt	0.00	0.00	0.00			0.00							
Au	0.00		0.01	0.01		0.00	0.00	0.01					
Fe	0.05	0.01	0.04	0.02	0.02	0.05	0.01	0.01	0.03	0.17	0.16	0.11	
Cu	0.06	0.31	0.07	0.05	0.33	0.19	0.08	0.09	0.04	0.18	0.09	0.29	
Pb	0.00	0.00		0.00				0.00			0.00	0.00	
As	3.74	3.64	3.74	3.72	3.59	3.67	3.67	3.69	3.69	3.67	3.65	3.62	4.00
Sb	0.00	0.00	0.01	0.01	0.01	0.01	0.00	0.00	0.01				
Te							0.09	0.12	0.07	0.00	0.08	0.03	

*Notes: Prefix 'gr.1' denotes grain 1, the largest grain of nipalarsite intergrown with isomertieite, sperrylite, hollingworthite and pentlandite (see Fig. 2e); 'gr.2' – grain 2 used for XRD analysis Fig. 2a,b; 'gr.3' – grain 3, nipalarsite studied with EBSD (Fig. 2c); 'gr.5' – grain 5, nipalarsite (studied with EBSD) intergrown with penlandite (Fig. 2d); 'Synth.' – synthetic analogue $\text{Ni}_8\text{Pd}_3\text{As}_4$, average of nine analyses on seven different grains. n.d. – not detected.

Table 4. Crystal data and structure refinement for the synthetic analogue of nipalarsite.

Crystal data	
Structural formula	Ni ₈ Pd ₃ As ₄
Crystal system, space group	cubic, <i>Fm</i> $\bar{3}$ <i>m</i>
<i>a</i> (Å)	11.4428(9)
<i>V</i> (Å ³)	1498.3(4)
<i>Z</i>	8
<i>D</i> _{calc} g/cm ³	9.65
μ (mm ⁻¹)	44.06
Data collection	
Diffractometer	Bruker APEX-II CCD
Radiation, wavelength (Å)	MoK α (λ = 0.71073)
Temperature (K)	293(2)
2 θ range for data collection (°)	3.08 to 32.48
<i>R</i> _{int} , <i>R</i> _{sigma} (%)	3.11, 0.61
Indices range of <i>h</i> , <i>k</i> , <i>l</i>	-17 ≤ <i>h</i> ≤ 17, -17 ≤ <i>k</i> ≤ 17, -17 ≤ <i>l</i> ≤ 17
Refinement	
No. of measured, independent and observed [<i>I</i> > 2 σ (<i>I</i>)] reflections	9957, 179, 175
Data/restraints/parameters	179/0/16
<i>S</i> (Goodness-of-fit on <i>F</i> ²)	1.439
<i>R</i> [<i>I</i> > 4 σ (<i>I</i>)]	<i>R</i> ₁ = 0.0144, <i>wR</i> ₂ = 0.0357
<i>R</i> [all data]	<i>R</i> ₁ = 0.0155, <i>wR</i> ₂ = 0.0384
$\delta\rho$ (max)/(min) (e ⁻ /Å ³)	1.177/-1.015

$$w = 1/[\sigma^2(F_o^2) + (0.0092P)^2 + 41.4800P] \text{ where } P = (F_o^2 + 2F_c^2)/3$$

Synthetic analogue

Several grains of nipalarsite were extracted from the polished sections and examined using single-crystal X-ray diffraction. However, they behaved like aggregates of several grains, showed Debye–Scherrer rings and proved to be unsuitable for structural analysis. Therefore, a fragment of a single crystal of synthetic Ni₈Pd₃As₄ was used for the structural study. The synthetic Ni₈Pd₃As₄ phase was prepared using the evacuated silica glass tube method. Pure elements: palladium (99.95%), nickel (99.999%) and arsenic (99.999%) were used as starting materials for the synthesis. The evacuated tube with its charge was sealed and then annealed at 900°C for 7 days. After cooling in a cold-water bath, the charge was ground into powder in acetone using an agate mortar, and mixed thoroughly to homogenise. The pulverised charge was sealed in an evacuated silica-glass tube again and reheated at 350°C for 60 days. The experimental product was rapidly quenched in cold water.

X-ray crystallography

Single-crystal X-ray diffraction

A fragment of the synthetic analogue of Ni₈Pd₃As₄ was examined using a Bruker Apex–II diffractometer equipped with a CCD detector (MoK α radiation). A total of 9957 reflections were collected. The data were integrated and corrected for Lorentz and

polarisation effects by means of the Bruker *S*AINT program. A semi-empirical absorption correction was applied on the basis of intensities of equivalent reflections using *S*ADABS (Sheldrick, 2008).

The crystal structure was solved *via* direct methods in the space group *Fm* $\bar{3}$ *m* and refined to the final *R* factor of 0.0144 (for 175 unique observed reflections with $|F| \geq 2\sigma F$). All calculations were performed with *S*HELX programs (Sheldrick, 2015a,b) in the framework of a *WinGX* software package (Farrugia, 2012).

All atomic positions were located by direct methods and subsequently refined anisotropically. Inspection of the difference-Fourier map revealed that maximum positive and negative peaks were 1.177 and -1.015 e⁻/Å³, respectively. The refinement yielded a relatively short Pd–As3 distance of 2.3698 Å within the [As3Pd₆] octahedra (see below). Refinement allowing the occupancy of As3 atom at the 4*b* position (½, ½, ½) to vary showed no tendency of this atom to depart from the full occupancy. Refinement with the disordered As3 atom at the adjacent 24*e* position (*x*, ½, ½) resulted in unacceptably short Pd–As3 contacts and is considered as less probable than the model with As3 at the 4*b* position. Details of data collection, crystallographic data and refinement are in Table 4. Atomic coordinates and anisotropic displacement parameters are presented in Table 5, respectively and interatomic distances are given in Table 6.

The crystallographic information files have been deposited with the Principal Editor of *Mineralogical Magazine* and are available as Supplementary material (see below).

Powder X-ray diffraction

Powder X-ray diffraction data of nipalarsite (Table 7) were obtained from an isolated grain (Fig. 2b) using a Rigaku R-AXIS Rapid II diffractometer equipped with a cylindrical image plate detector, in Debye–Scherrer geometry (*d* = 127.4 mm; CoK α radiation). The data were integrated using the software package *OSC2XRD* (Britvin et al., 2017). As only a few reflections were detected the unit-cell refinement was performed on the synthetic material.

Powder X-ray diffraction data of the synthetic analogue of nipalarsite were collected on a Bruker D8 Advance diffractometer using CuK α radiation and the LynxEye XE detector in Bragg–Brentano geometry. The data were indexed by means of the structure model derived from the single-crystal diffraction data (see above). The unit-cell refinement was performed by the *CelRef* program (Laugier and Boch, 2003), yielding refined unit-cell parameters of *a* = 11.4352(6) Å and *V* = 1495.3 Å³.

Description of the crystal structure

The crystal structure of nipalarsite (Fig. 4) contains two Ni atom positions (both at Wyckoff position 32*f*), one Pd atom position

Table 5. Atomic coordinates and equivalent isotropic and anisotropic displacement parameters (Å²) for the synthetic analogue of nipalarsite.

Atom	Wyck. symbol	<i>x</i>	<i>y</i>	<i>z</i>	Occ.	<i>U</i> _{eq}	<i>U</i> ¹¹	<i>U</i> ²²	<i>U</i> ³³	<i>U</i> ²³	<i>U</i> ¹³	<i>U</i> ¹²
Pd1	24 <i>e</i>	0.29290(7)	0	0	1	0.0167(2)	0.0198(4)	0.0151(2)	0.0151(2)	0	0	0
As1	4 <i>a</i>	0	0	0	1	0.0059(3)	0.0059(3)	0.0059(3)	0.0059(3)	0	0	0
As2	24 <i>d</i>	0	¼	¼	1	0.0079(2)	0.0092(2)	0.0092(2)	0.0054(3)	0	0	0.0001(3)
Ni1	32 <i>f</i>	0.38240(5)	0.11760(5)	0.38240(5)	1	0.0094(2)	0.0094(2)	0.0094(2)	0.0094(2)	0.0016(2)	-0.0016(2)	0.0016(2)
Ni2	32 <i>f</i>	0.33429(5)	0.33429(5)	0.66571(5)	1	0.0123(2)	0.0123(2)	0.0123(2)	0.0123(2)	-0.0047(2)	-0.0047(2)	0.0047(2)
As3	4 <i>b</i>	½	½	½	1	0.0376(8)	0.0376(8)	0.0376(8)	0.0376(8)	0	0	0

Table 6. Selected interatomic distances (Å) in the structure of the synthetic analogue of nipalarsite.

Pd1–As3	2.3698(8)	Ni1–As1	2.3309(9)
Pd1–Ni2	2.7231(8) ×4	Ni1–As2	2.5301(4) ×2
Pd1–Ni1	2.7650(6) ×4	Ni1–Ni2	2.5988(8) ×3
Pd1–As2	2.9025(3) ×3	Ni1–Ni1	2.6915(11) ×3
		Ni1–Pd1	2.7650(6) ×2
As1–Ni1	2.3309(9) ×8		
As2–Ni2	2.3358(2) ×4	Ni2–As2	2.3358(2) ×3
As2–Ni1	2.5301(4) ×4	Ni2–Ni1	2.5988(8) ×3
As2–Pd1	2.9025(3) ×4	Ni2–Pd1	2.7231(8) ×3
		Ni2–Ni2	2.7280(18) ×3
As3–Pd1	2.3698(8) ×6		

Table 7. Powder X-ray diffraction data (d in Å) obtained from nipalarsite and its synthetic analogue.

Nipalarsite – natural material ¹				Synthetic analogue ²			
l_{obs}	d_{obs}	d_{calc}	$h k l$	l_{obs}	d_{obs}	d_{calc}	$h k l$
				2	5.7175	5.7175	0 0 2
				10	2.8590	2.8588	0 0 4
				6	2.6234	2.6234	3 1 3
				6	2.5572	2.557	0 2 4
				11	2.3343	2.3342	2 2 4
48	2.21	2.2	1 1 5, 3 3 3	35	2.2007	2.2007	1 1 5, 3 3 3
100	2.03	2.02	0 4 4	100	2.0215	2.0215	0 4 4
				6	1.9327	1.9329	1 3 5
6	1.91	1.91	0 0 6, 2 4 4	8	1.9058	1.9058	0 0 6, 2 4 4
				3	1.808	1.808	2 0 6
				3	1.7438	1.7438	3 3 5
				6	1.724	1.7239	2 2 6
				1	1.6012	1.6012	1 1 7
				6	1.4887	1.4887	1 3 7
				7	1.4293	1.4294	0 0 8
				4	1.3477	1.3476	6 0 6
				1	1.3204	1.3204	5 1 7

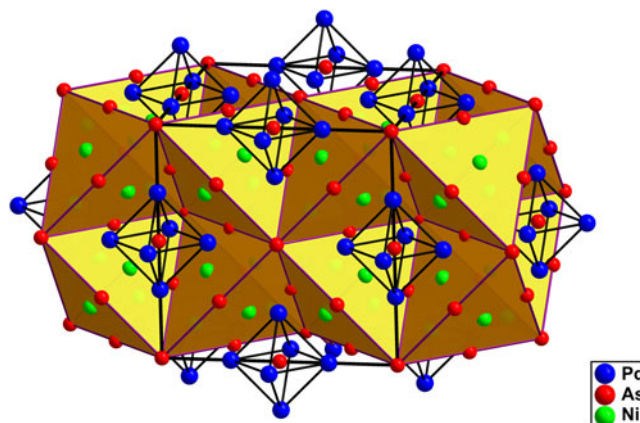
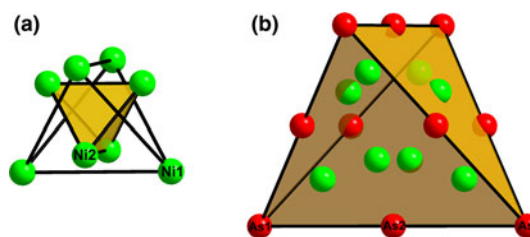
¹Obtained by Rigaku R-AXIS Rapid II diffractometer equipped with a cylindrical image plate detector, Debye-Scherrer geometry ($d = 127.4$ mm; $\text{CoK}\alpha$ radiation).

²Powder diffractometer in Bragg-Brentano geometry, $\text{CuK}\alpha$ radiation.

(Wyckoff 24e), and three As atom positions (Wyckoff 4a, 24d and 4b). This yields 120 atoms within a unit-cell and the formula $\text{Ni}_8\text{Pd}_3\text{As}_4$ for $Z = 8$.

As is typical for intermetallic phases, the nipalarsite crystal structure is characterised by atoms with complex coordination environments and high coordination numbers. Ni1 is coordinated by 13 atoms (4 As, 7 Ni and 3 Pd), while the Ni2 atom has a coordination number of 12 (3 As, 6 Ni and 3 Pd). Ni1–As distances are in the range 2.3309–2.5301 Å. Ni2–As distances are equal to 2.3358 Å. Ni–Ni distances vary between 2.5988 Å and 2.7280 Å. Pd atoms show 4+4 Ni contacts at distances of 2.7231 Å and 2.7650 Å, respectively. The Pd coordination is completed by three As2 atoms at 2.9025 Å and a short distance to the As3 site (2.3698 Å).

The crystal structure of nipalarsite can be considered as a stuffed derivative of the $\text{Mg}_6\text{Cu}_{16}\text{Si}_7$ structure type (Bergmann and Waugh, 1956), which is also referred to as the $\text{Th}_6\text{Mn}_{23}$ structure type in the Inorganic Crystal Structure Database (Fachinformationszentrum Karlsruhe, 2018). Considering this relation, the nipalarsite chemical composition can be expressed as $\text{Pd}_6\text{Ni}_{16}\text{As}_7\text{As}_1$ (for $Z = 4$), which is directly comparable to that of $\text{Mg}_6\text{Cu}_{16}\text{Si}_7(\square)$, where \square = vacancy. In nipalarsite, As3 atoms occupy the 4b position of the space group $Fm\bar{3}m$. This position is empty in the $\text{Mg}_6\text{Cu}_{16}\text{Si}_7$ structure type.

**Fig. 4.** Crystal structure of nipalarsite showing the edge-sharing framework of $[\text{Ni}_8\text{As}_{10}]$ supertetrahedra. The $[\text{As}_3\text{Pd}_6]$ octahedra are emphasised.**Fig. 5.** Detailed view of (a) the Ni_8 cluster and (b) the $[\text{Ni}_8\text{As}_{10}]$ supertetrahedra in the nipalarsite crystal structure.

Nipalarsite is an intermetallic phase and its structural arrangement is not easy to visualise. As was mentioned by Holman *et al.* (2008) for synthetic phases with the $\text{Mg}_6\text{Ni}_{16}\text{Si}_7$ structure type, such structures can be described conveniently in terms of large intermetallic polyhedra. The nipalarsite structure contains a cluster of eight Ni atoms formed from two interpenetrating Ni_4 tetrahedra (Fig. 5a). As is indicated in Fig. 5b, this cluster is subsequently surrounded by 10 As atoms forming the $[\text{Ni}_8\text{As}_{10}]$ supertetrahedra, which can be selected as a basic structural motive used for a structural description. The nipalarsite structure can be then viewed as an edge-sharing framework of the $[\text{Ni}_8\text{As}_{10}]$ supertetrahedra (Fig. 4). An important feature of this structural arrangement is the presence of large structural cavities. These cavities contain the Pd_6 octahedra with As3 atoms at their centres. The Pd–As3 distance of 2.3698 Å in this regular $[\text{As}(3)\text{Pd}_6]$ octahedra is slightly shorter than similar Pd–As contacts in Pd-bearing arsenides (e.g. 2.425 Å in PdAs_2 , Furuseth *et al.*, 1967), however it seems to be a feature of the nipalarsite structure. Similar short bonding distances were observed in crystal structures of polar intermetallic phases (e.g. Ca–Ca in CaAu_3Ga , Lin and Corbett, 2008; Ag–Ag in AgPd_3Se , Laufek *et al.*, 2011), very likely to be because of the matrix effect of surrounding atoms. The filler atoms do not have enough space to expand the network and hence short bonds occur.

Nipalarsite does not have a structural analogue in the mineralogical system. From a chemical point of view, the most related minerals are majakite, PdNiAs , (Evstigneeva *et al.*, 2000) and menshikovite, $\text{Pd}_3\text{Ni}_2\text{As}_3$ (Barkov *et al.*, 2002). The majakite structure is based on $[\text{PdAs}_5]$ square pyramids and $[\text{NiAs}_4]$ distorted tetrahedra, the nipalarsite structure is typical for

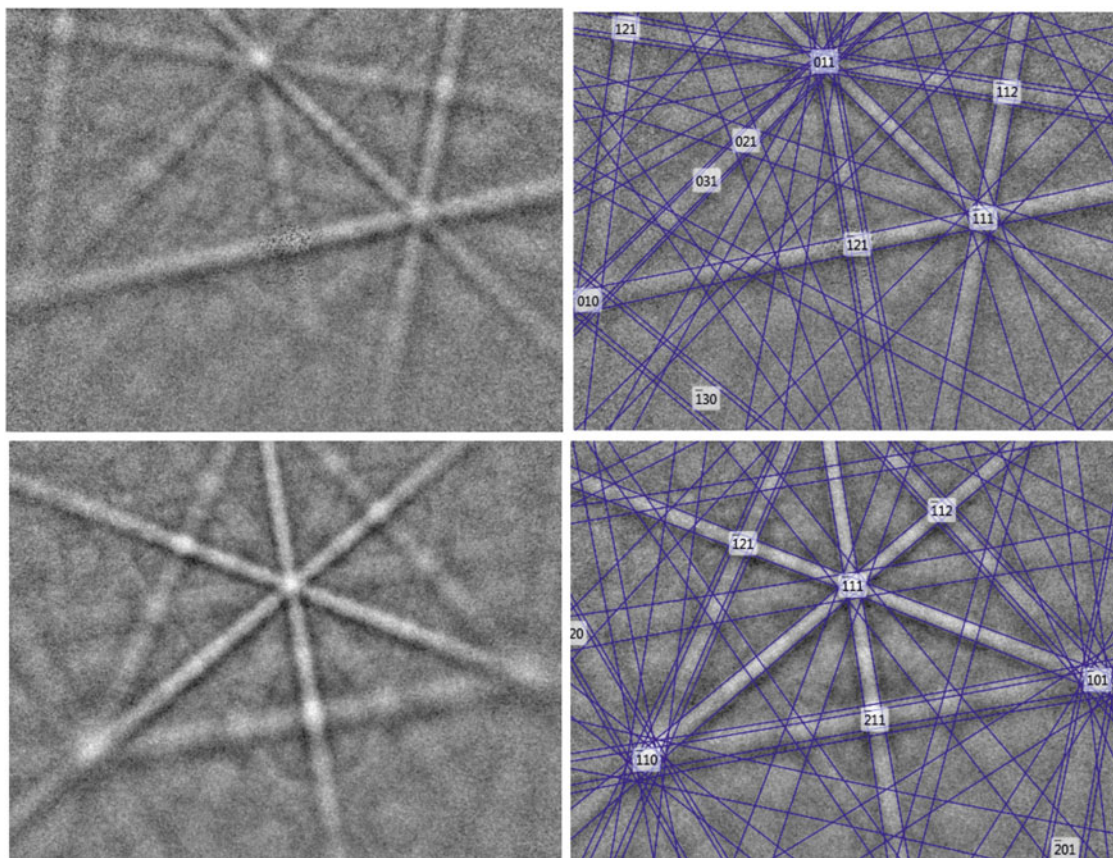


Fig. 6. EBSD image of natural nivalarsite; in the right pane, the Kikuchi bands are indexed.

intermetallic compounds with high coordination numbers and hence is very different from that of majakite. The crystal structure of menshikovite is not known.

Relation of nivalarsite to synthetic $\text{Ni}_8\text{Pd}_3\text{As}_4$

The structural identity of the natural and synthetic phase was confirmed by electron back-scattered diffraction (EBSD) measurements on the natural sample (grains in Fig. 2c,d) and comparison of X-ray diffraction data obtained from natural and synthetic $\text{Ni}_8\text{Pd}_3\text{As}_4$.

The collected diffraction data from natural nivalarsite fit very well to those of synthetic $\text{Ni}_8\text{Pd}_3\text{As}_4$ (Table 7). Moreover, the EBSD patterns (also known as Kikuchi patterns) derived from the crystal structure of $\text{Ni}_8\text{Pd}_3\text{As}_4$ phase, fit very well to the measured patterns obtained from the natural grains of nivalarsite. The natural sample was prepared for investigation by etching the mechanically polished surface with colloidal silica (OP-U) for 15 min. to reduce the surface damage. The EBSD patterns were collected and processed using the proprietary computer program *AZtec HKL* (Oxford Instruments). The values of the mean angular deviation (MAD, i.e. goodness of fit of the solution) between the calculated and measured Kikuchi bands range between 0.53° and 0.39° . These values reveal a very good match; as long as values of mean angular deviation are <1 , they are considered as indicators of an acceptable fit. A TESCAN Mira 3GMU scanning electron microscope combined with an EBSD system (Nordlys Nano detector, Oxford Instruments) was used for the measurements. The solid angles calculated from the patterns were compared with a structural

model proposed match containing 90 reflectors to index the patterns. The EBSD patterns obtained from the natural material (18 measurements on different spots on natural nivalarsite) were found to match the patterns generated from our structural model (Fig. 6).

Genetic implications and conclusions

Nivalarsite was found in association with other PGMs, disseminated sulfides and hydrous silicates in the intercumulus of orthopyroxene and plagioclase. It crystallised in intergrowths with isomertieite, hollingworthite, other PGMs and pentlandite. In some cases, nivalarsite replaces symplectites of menshikovite and pentlandite.

The Pd–Ni–As system was studied experimentally at 450°C and 790°C by Gervilla *et al.* (1994). The existence of many binary and only two ternary compounds was established at 450°C , PdNiAs (majakite) and $\text{Pd}_3\text{Ni}_2\text{As}_3$ (menschikovite). Nivalarsite was not observed at 450°C or at higher temperatures investigated by Gervilla *et al.* (1994). It is likely that the solid solution of stillwaterite (Pd_8As_3) dissolving Ni (observed by Gervilla *et al.*, 1994) breaks down at lower temperatures and nivalarsite is formed. The synthetic analogue of nivalarsite was synthesised for this study at 350°C . Apparently its temperature of formation is lower than that of majakite and menshikovite, which is confirmed by the mineral association, where menshikovite and pentlandite form symplectites replaced by nivalarsite. Consequently, the proposed new mineral was probably formed in post magmatic, hydrothermal conditions at lower temperatures, equal or below 350°C .

However, its occurrence at higher temperatures under different thermodynamic conditions is not excluded.

Supplementary material. To view supplementary material for this article, please visit <https://doi.org/10.1180/mgm.2019.70>

Acknowledgements. The authors acknowledge Ulf Hälenius, Chairman of the CNMNC and its members for helpful comments on the submitted data. Constructive comments made by Louis J. Cabri, Andrei Barkov, an anonymous reviewer and Structures Editor Peter Leverett are greatly appreciated; they improved the quality of the manuscript. The editorial handling by Stuart Mills is also acknowledged. We thank Dr. A.A. Zolotarev (XRD Center of the St. Petersburg State University) for the help in collection of the single-crystal XRD data. This study was supported by the Russian Academy of Sciences, Program of Fundamental Research and by the Grant Agency of the Czech Republic (Project no. 18-15390S to AV). The work of DAC is supported by Act 211 Government of the Russian Federation, agreement No.02.A03.21.0006 and is performed according to the Russian Government Program of Competitive Growth of Kazan Federal University.

References

- Amelin Yu.V., Heaman L.M. and Semenov V.S. (1995) U–Pb geochronology of layered mafic intrusions in the Eastern Baltic Shield – implications for the timing and duration of Paleoproterozoic continental rifting. *Precambrian Research*, **75**, 31–46.
- Barkov A.Y., Martin R.F., Pakhomovsky Y.A., Tolstykh N.D. and Krivenko A.P. (2002) Menshikovite, Pd₃Ni₂As₃, a new platinum-group mineral species from two layered complexes, Russia. *The Canadian Mineralogist*, **40**, 679–692.
- Bayanova T.B., Nerovich L.I., Mitrofanov F.P., Zhavkov V.A. and Serov P.A. (2010) The Monchetundra Basic Massif of the Kola Region: New Geological and Isotope Geochronological Data. *Doklady Earth Sciences*, **431**, 288–293.
- Bergman G. and Waugh J.L.T. (1956) The crystal structure of the intermetallic compound Mg₆Si₇Cu₁₆. *Acta Crystallographica*, **9**, 214–217.
- Britvin S.N., Dolivo-Dobrovolsky D.V. and Krzhizhanovskaya M.G. (2017) Software for processing of X-ray powder diffraction data obtained from the curved image plate detector of Rigaku RAXIS Rapid II diffractometer. *Proceedings of the Russian Mineralogical Society*, **146**, 104–107 [in Russian].
- Evstigneeva T., Kabalov Yu. and Schneider J. (2000) Crystal structure of NiPdAs, ordered member of isomorphous series Pd₂As–Ni₂As. *Materials Science Forum*, **321–324**, 700–704.
- Fachinformationszentrum Karlsruhe (2018) *Inorganic Crystal Structure Database*. Karlsruhe, Germany.
- Farrugia L.J. (2012) WinGX and ORTEP for Windows: an update. *Journal of Applied Crystallography*, **45**, 849–854.
- Furuseth S.; Selte K., Kjekshus A. (1967) On the solid solubility and structural properties of PdAs_{2-x}Sb_x, PtP_{2-x}As_x, PtP_{2-x}Sb_x, PtP_{2-x}Bi_x, PtAs_{2-x}Sb_x, PtAs_{2-x}Bi_x, PtSb_{2-x}Bi_x, Pd_{1-m}Pt_mAs₂, Pd_{1-m}Pt_mSb₂, Pd_{1-m}Au_mSb₂, and Pt_{1-m}Au_mSb₂. *Acta Chemica Scandinavica*, **21**, 527–536.
- Genkin A.D. and Evstigneeva T.L. (1986) Association of platinum-group minerals of the Noril'sk copper-nickel sulfide ores. *Economic Geology*, **81**, 1203–1212.
- Genkin A.D., Distler V.V., Gladyshev G.D., Filimonova A., Evstigneeva T.L., Kovalenker V.A., Laputina I. P., Smirnov A.V. and Grokhovskaya T.L. (1981) *Sulfide copper-nickel ores of Norilsk deposits*. Moscow, Nauka, 234 pp. [in Russian].
- Gervilla F., Makovicky E., Makovicky M. and Rose-Hansen J. (1994) The system Pd–Ni–As at 790° and 450° C. *Economic Geology*, **89**, 1630–9.
- Grokhovskaya T.L., Bakaev G.F., Sholokhnev V.V., Lapina M.I. and Muravitskaya G.N. (2003) The PGE Ore mineralization in the Monchegorsk Igneous Layered Complex (Kola Peninsula, Russia). *Geology of Ore Deposits*, **45**, 287–309.
- Grokhovskaya T.L., Lapina M.I. and Mokhov A.V. (2009) Assemblages and genesis of platinum-group minerals in low-sulfide ores of the Monchetundra deposit, Kola Peninsula, Russia. *Geology of Ore Deposits*, **51**, 467–485.
- Grokhovskaya T., Karimova O., Vymazalová A., Laufek F., Chareev D. and Rassulov V. (2018) Nipalarsite, IMA 2018–075. CNMNC Newsletter No. 46, December 2018, page 1370; *Mineralogical Magazine*, **82**, 1369–1379.
- Holman K.L., Morosan E., Casey P.A., Li L., Ong N.P., Klimczuk T., Felser C. and Cava R.J. (2008) Crystal structure and physical properties of Mg₆Cu₁₆Si₇-type M₆Ni₁₆Si₇, for M = Mg, Sc, Ti, Nb and Ta. *Materials Research Bulletin*, **43**, 9–15.
- Laufek F., Vymazalova A.; Chareev D.A., Kristavchuk A.V., Lin Q., Drahokoupil J., Vasilchikova T.M. (2011) Crystal and electronic structure study of AgPd₃Se. *Journal of Solid State Chemistry*, **184**, 2794–2798.
- Laugier J. and Bochu B. (2003) *CELREF: Unit Cell Refinement Program from Powder Diffraction Diagram*. Laboratoires des Matériaux et du Génie Physique, Ecole Nationale Supérieure de Physique de Grenoble (INPG), Grenoble, France.
- Lin Q. and Corbett J.D. (2008) Interpenetrating networks of three-dimensional Penrose tiles in CaAu₃Ga, the structurally simplest cubic approximant of an icosahedral quasicrystal. *Inorganic Chemistry*, **47**, 3462–3464.
- Sheldrick G.M. (2008) A short history of SHELX. *Acta Crystallographica*, **A64**, 112–122.
- Sheldrick G.M. (2015a) *SHELXT* – Integrated space-group and crystal structure determination. *Acta Crystallographica*, **A71**, 3–8.
- Sheldrick G.M. (2015b) Crystal structure refinement with *SHELXL*. *Acta Crystallographica*, **C71**, 3–8.